Nuclear Science and Techniques (2025) 36:241
https://doi.org/10.1007/s41365-025-01827-9

Microscopic calculation of photon strength functions in Nd isotopes using the dirac quasiparticle finite amplitude method

Hai-Ruo Liu[1] · Yuan Tian[1] · Rui-Rui Xu[1] · Yi-Fei Niu[2] · Ying Cui[3] · Xi Tao[1] · Xiao-Dong Sun[1] · Zhi Zhang[1] · Zhi-Gang Ge[1] · Neng-Chuan Shu[1]

Received: 27 February 2025 / Revised: 15 March 2025 / Accepted: 22 March 2025 / Published online: 17 October 2025

Abstract

In this study, we calculated the photon absorption cross sections of even–even neodymium (Nd) isotopes using the Dirac Quasiparticle Finite Amplitude Method (relativistic QFAM), combined with the Tiny Smearing Approximation (TSA) method. This approach enables the efficient reproduction of experimental photon absorption data for both spherical and deformed nuclei. We demonstrate that relativistic QFAM calculations with any smearing parameter γ can be scaled using the TSA method, significantly reducing the computational cost. Our method was applied to Nd isotopes, with experimental data reproduced for ^{142,144,146,148,150}Nd and predictions for ^{152}Nd. By optimizing the three key parameters, the total χ^2 between the calculations and experimental data was reduced by nearly an order of magnitude. Furthermore, the role of nuclear deformation in the Giant Dipole Resonance (GDR) structure was analyzed, highlighting its impact on the emergence of double peaks in the photon absorption cross sections of deformed nuclei. This work provides a robust microscopic approach to improve photonuclear data for applications in nuclear physics and astrophysics.

Keywords Relativistic mean field · Relativistic quasiparticle finite amplitude method · Photon–nuclear reaction · Photon absorption cross section

1 Introduction

Neodymium isotopes play a crucial role in nuclear processes. They are important fission products that are widely used in activation analysis and reactor physics research [1–3]. Their neutron capture and photonuclear properties affect key areas of nuclear science, including neutron economy [4], fuel cycle management [5], radiation shielding [6], and nuclear astrophysics [7]. Neodymium has seven naturally stable isotopes, namely, ^{142,143,144,145,146,148,150}Nd, with abundances of 27.15%, 12.17%, 23.798%, 23.798%, 8.293%, 17.189%, and 5.638%, respectively [3]. Accurate knowledge of their photonuclear cross sections is essential for enhancing fission reactor modeling, activation analysis, and broader applications, such as reactor design and nucleosynthesis studies.

Early studies of photonuclear reactions used broad-spectrum bremsstrahlung light sources from electron linear accelerators and quasi-monochromatic positron annihilation sources based on time-of-flight methods [8]. Between 1962 and 1987, the Lawrence Livermore National Laboratory [9] and the Saclay Laboratory [10] conducted numerous

This work was supported by the National Key Research and Development (R&D) Program (Nos. 2022YFA1602403, 2021YFA1601500), Key Program of the National Natural Science Foundation of China (No.12435007), the National Natural Science Foundation of China (Nos.12075104, 12447106, and 12147101), the Basic Research Project of China National Nuclear Corporation (CNNC) (No. CNDC-JCYJ-202402), CNNC Youth Innovation Team Project Key Laboratory Fund, the Key Laboratory Fund Key Projects (No. JCKY2023201C153-5), and Continuous Support Basic Scientific Research Project (BJ010261223282).

✉ Yuan Tian
tiany@ciae.ac.cn

✉ Rui-Rui Xu
xuruirui@ciae.ac.cn

✉ Yi-Fei Niu
niuyf@lzu.edu.cn

[1] China Nuclear Data Center, China Institute of Atomic Energy, P.O. Box 275(10), 102413 Beijing, China

[2] School of Nuclear Science and Technology, Lanzhou University, Lanzhou 730000, China

[3] China Institute of Atomic Energy, P.O. Box 275(10), Beijing 102413, China

experiments using quasi-monochromatic light sources, yielding precise photoneutron cross section data. However, Berman's review highlighted discrepancies between the (γ,n) and (γ,2n) cross sections from the two laboratories, emphasizing the need for further investigation.

New photonuclear reaction data have been obtained through experiments at facilities such as NewSUBARU and Oslo [11]. Advances in light source and neutron detection technologies have led to the development of high-quality experimental facilities. Recently, the Shanghai Advanced Research Institute completed an SLEGS facility using inverse Compton backscattering [12], which has attracted significant attention. The China Nuclear Data Center (CNDC) collaborates with the SLEGS facility to improve measurement techniques and theoretical evaluations with the goal of establishing a comprehensive photonuclear reaction database.

To enhance the quality of photonuclear reaction cross section data and resolve inconsistencies, the International Atomic Energy Agency (IAEA) has organized two Coordinated Research Projects (CRPs) on photonuclear reactions. A recent CRP, conducted from 2016 to 2020, updated the IAEA's photonuclear data and established a reference database for photon strength functions (PSF) [13–15]. The CNDC actively participated in both the CRPs, making significant contributions through experimental evaluations and theoretical calculations.

In theoretical approaches, two types of models are used to predict the strength function: phenomenological models and microscopic models [16–21]. The most commonly used phenomenological models include the Standard Lorentzian (SLO) model [22, 23], Enhanced Generalized Lorentzian (EGLO) model [24, 25], and Generalized Fermi-Liquid (GFL) model [26]. Microscopic models encompass the Finite Fermi Gas theory [27, 28], semi-classical thermodynamic approach [29], non-relativistic Quasiparticle Random Phase Approximation (QRPA) based on the BCS ground state [30], and relativistic Quasi-Particle Random Phase Approximation (RQRPA) based on the covariant density functional theory [31–33]. Phenomenological methods usually rely heavily on large amounts of experimental data; however, there are conflicts between the data measured by the Saclay Laboratory and the Livermore National Laboratory. Therefore, microscopic methods are required for this purpose.

QRPA has been the most popular microscopic method. The QRPA and RQRPA methods have been successful for spherical nuclei; however, for deformed nuclei, the QRPA matrix becomes large, requiring significant computational and storage resources [34]. To address this, the finite amplitude method (FAM) was introduced, which avoids the construction and diagonalization of the full QRPA matrix. Instead, FAM iteratively solves the linear response problem by calculating the fields excited by the one-body transition operators [35–37]. In 2020, A. Bjelcic and T. Niksic developed a QFAM model based on relativistic EDFs (DIRQFAM program) to compute the multipole response of even–even deformed nuclei [38], and in 2023, DIRQFAM2.0 was released with updates including meson exchange interactions and a new solver method [39].

The aim of this work is to better describe the experimental photon absorption cross section using the microscopic method, as the photon absorption cross section calculated by QFAM still shows a significant discrepancy with the experimental results. In this study, we calculated the photon absorption cross sections of even–even Nd isotopes using DIRQFAM2.0 and compare the results with experimental data. Section 2 outlines the theoretical framework of relativistics and introduces an approximation method for optimizing the system to align it with the experimental data. In Sect. 3, we discuss our results in detail. Finally, Section 4 presents the conclusions and future prospects of this study.

2 Theoretical framework

The theoretical photoabsorption cross section $\sigma_{\rm abs}(\epsilon_\gamma)$ as a function of gamma ray energy ϵ_γ is taken as the sum of the terms

$$\sigma_{\rm abs}(\epsilon_\gamma) = \sigma_{\rm GDR}(\epsilon_\gamma) + \sigma_{\rm QD}(\epsilon_\gamma), \tag{1}$$

where the component $\sigma_{\rm GDR}(\epsilon_\gamma)$ corresponds to the excitation of the GDR and $\sigma_{\rm QD}(\epsilon_\gamma)$ is a quasideuteron contribution (a photoabsorption by a neutron–proton pair), which is taken in accordance with the model proposed by Chadwick et al. [40, 41].

The GDR component $\sigma_{\rm GDR}(\epsilon_\gamma)$ of the total photoabsorption cross section is equal to that of the electric dipole gamma rays $\sigma_{E1}(\epsilon_\gamma)$, which is proportional to the strength function $R_{E1}(\epsilon_\gamma)$

$$\sigma_{E1}(\epsilon_\gamma) = \frac{16\pi^3}{9}\frac{e^2}{\hbar c}\epsilon_\gamma R_{E1}(\epsilon_\gamma), \tag{2}$$

where the isovector dipole strength function $R_{E1}(E_\gamma)$ can be calculated using a microscopic model, such as the RQRPA equations [31, 42–44]. In standard notation, these equations can be written in matrix form as

$$\begin{pmatrix} A^J & B^J \\ B^{*J} & A^{*J} \end{pmatrix}\begin{pmatrix} X^{\nu J} \\ Y^{\nu J} \end{pmatrix} = \omega^\nu \begin{pmatrix} 1 & 0 \\ 0 & -1 \end{pmatrix}\begin{pmatrix} X^{\nu J} \\ Y^{\nu J} \end{pmatrix}. \tag{3}$$

For each RQRPA energy, ω^ν, X^ν, and Y^ν denote the corresponding forward- and backward-going two-quasiparticle amplitudes, respectively.

The RQRPA equation can be solved by directly diagonalizing the A and B matrices (3) for the spherical nuclei.

However, for deformed systems, the dimensionality of these matrices increases rapidly, and such calculations were only possible approximately a decade ago [45, 46]. To overcome the challenges of implementing matrix-based RPA for deformed heavy nuclei, FAM was introduced as an efficient alternative for calculating the multipole response functions. FAM has been successfully applied in numerous studies, both in coordinate space and on the harmonic oscillator basis [38, 39, 47, 48].

2.1 Relativistic QFAM

The ground-state properties of the nuclei were determined within the framework of the Relativistic Hartree–Bogoliubov (RHB) method. The RHB Hamiltonian incorporates the mean-field term $\hat{h}$ which accounts for long-range particle-hole correlations, and the pairing field Δ which describes particle-particle correlations. The RHB equation was formulated as follows:

$$\begin{pmatrix} \hat{h}-m-\lambda & \hat{\Delta} \\ -\hat{\Delta}^* & -\hat{h}^*+m+\lambda \end{pmatrix}\begin{pmatrix} U_k \\ V_k \end{pmatrix} = E_k \begin{pmatrix} U_k \\ V_k \end{pmatrix}. \tag{4}$$

In this study, the RHB calculations were performed self-consistently using the DD-PC1 relativistic density functional [49] along with a separable pairing interaction. The pairing force in momentum space is expressed as

$$kV_{\text{sep}}^{^1S_0}k' = -Gp(k)p\left(k'\right), \tag{5}$$

where the pairing form factor $p(k)$ is assumed to have a Gaussian shape, $p(k) = e^{-\alpha^2 k^2}$. By fitting the parameters G and α to reproduce the results of the Gogny D1S interaction, the values were determined to be $G = 728$ MeV fm^3 and $\alpha = 0.644$ fm [44, 50].

The Giant Dipole Resonance (GDR) strength is given by the relativistic QFAM equation, which describes the nuclear response to an external one-body field $\hat{F}(t) = \eta\left\{\hat{F}e^{-i\omega t} + \hat{F}^\dagger e^{i\omega t}\right\}$ oscillating with a frequency ω in the small amplitude limit,

$$\begin{aligned} (E_\mu + E_\nu - \omega)X_{\mu\nu}(\omega) + \delta H^{20}_{\mu\nu}(\omega) &= F^{20}_{\mu\nu}(\omega), \\ (E_\mu + E_\nu + \omega)Y_{\mu\nu}(\omega) + \delta H^{02}_{\mu\nu}(\omega) &= F^{02}_{\mu\nu}(\omega), \end{aligned} \tag{6}$$

where E_μ and E_ν are the one-quasiparticle energy, $F^{20}_{\mu\nu}$ and $F^{02}_{\mu\nu}$ represent the coefficients of the components of $\hat{F}$ expanded by the two-quasiparticle operators $\hat{a}^\dagger_\mu\hat{a}^\dagger_\nu$ and $\hat{a}^\dagger_\mu\hat{a}^\dagger_\nu$, respectively, and $\delta H^{20}_{\mu\nu}$ and $\delta H^{02}_{\mu\nu}$ are the coefficients of the components of $\delta\hat{H}(\omega)$ expanded by the two-quasiparticle operators operator $\hat{a}^\dagger_\mu\hat{a}^\dagger_\nu$ and $\hat{a}^\dagger_\mu\hat{a}^\dagger_\nu$, respectively. By expanding δH^{20} and δH^{02} in terms of $X(\omega)$ and $Y(\omega)$, we obtain:

$$\begin{aligned} \delta H^{20}_{\mu\nu}(\omega) &= \sum_{\mu'<\nu'} \left\{A_{\mu\nu,\mu'\nu'} - (E_\mu + E_\nu)\delta_{\mu\mu'}\delta_{\nu\nu'}\right\}X_{\mu'\nu'}(\omega) \\ &\quad + \sum_{\mu'<\nu'} B_{\mu\nu,\mu'\nu'}Y_{\mu'\nu'}(\omega), \\ \delta H^{02}_{\mu\nu}(\omega) &= \sum_{\mu'<\nu'} \left\{A^*_{\mu\nu,\mu'\nu'} - (E_\mu + E_\nu)\delta_{\mu\mu'}\delta_{\nu\nu'}\right\}X_{\mu'\nu'}(\omega) \\ &\quad + \sum_{\mu'<\nu'} B^*_{\mu\nu,\mu'\nu'}Y_{\mu'\nu'}(\omega), \end{aligned} \tag{7}$$

where A and B are the usual RQRPA matrices [32] and the linear response equation becomes

$$\left[\begin{pmatrix} A & B \\ B^* & A^* \end{pmatrix} - \omega\begin{pmatrix} 1 & 0 \\ 0 & -1 \end{pmatrix}\right]\begin{pmatrix} X(\omega) \\ Y(\omega) \end{pmatrix} = -\begin{pmatrix} F^{20} \\ F^{02} \end{pmatrix}. \tag{8}$$

Thus, the relativistic QFAM equations are equivalent to linear response formalism. Furthermore, when the right-hand side of Eq. (8) is zero, the relativistic QFAM equation leads to the conventional RQRPA Eq. (3).

2.2 Tiny smearing approximation method

While the relativistic QFAM approach offers a highly efficient solution to the standard RQRPA problem, it does not provide direct access to the RQRPA eigenfrequencies Ω_i However, the method proposed in Ref. [51], which is based on contour integration in a complex plane, enables the extraction of RQRPA transition matrix elements and eigenfrequencies from relativistic QFAM calculations.

In this section, the TSA method is introduced, which provides an efficient approach for connecting the relativistic QFAM strength function with the RQRPA transition matrix elements. As is well known, the response function is

$$R(\omega) = \frac{\mathrm{d}B(\omega)}{\mathrm{d}\omega} = \sum_i |\langle i|\hat{F}|0\rangle|^2 \frac{\gamma/\pi}{(\omega-\Omega_i)^2+\gamma^2}, \tag{9}$$

where $\mathrm{d}B(\omega)/\mathrm{d}\omega$ is the strength function of the relativistic QFAM, $|\langle i|\hat{F}|0\rangle|^2$ is the RQRPA transition matrix elements, and Ω_i is the eigenfrequency. If γ is sufficiently small, such as $\gamma = 0.01$ MeV, when $\omega = \Omega_k$,

$$\sum_i \frac{|\langle i|\hat{F}|0\rangle|^2}{(\omega-\Omega_i)^2+\gamma^2} \approx |\langle k|\hat{F}|0\rangle|^2 \frac{1}{\gamma^2} \tag{10}$$

becomes extremely larger, therefore, the transition matrix elements of the RQRPA can be approximated by

$$\left|\left\langle i\middle|\hat{F}\middle|0\right\rangle\right|^2 \approx \left.\frac{\mathrm{d}B(\omega)}{\mathrm{d}\omega}\pi\gamma\right|_{\omega=\Omega_i,\gamma=0.01}. \tag{11}$$

In Fig. 1, we present the isovector Giant Dipole Resonance (GDR) response of ^{142}Nd, calculated using DD-PC1

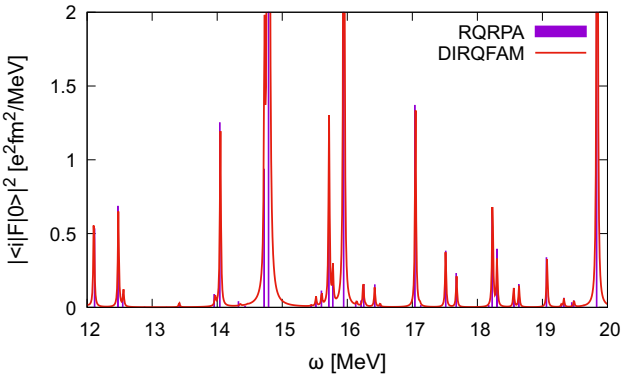

Fig. 1 (Color online) Isovector Giant dipole response of ^{142}Nd calculated using the DD-PC1 parameterization with a separable pairing interaction and N_{shells}=20 oscillator shells. The purple columns represent the results obtained from spherical RQRPA calculations, while the red curve corresponds to the relativistic QFAM calculations

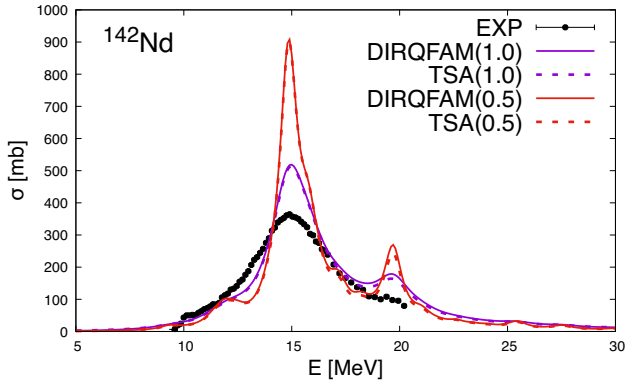

Fig. 2 (Color online) Comparison of the photon absorption cross section for ^{142}Nd calculated by relativistic QFAM (solid lines) using γ =0.5 and γ=1.0 MeV with TSA results (dashed lines) using γ=0.01 MeV. The black dots are the experimental data

parameterization with a separable pairing interaction and N_{shells}=20 oscillator shells. The purple columns represent the $|\langle i|\hat{F}|0\rangle|^2$ obtained from the spherical RQRPA calculations, whereas the red curve corresponds to the relativistic QFAM results for $\pi\gamma \mathrm{d}B(\omega)/\mathrm{d}\omega$ calculated with a smearing parameter of $\gamma = 0.01$ MeV. This comparison demonstrated that Eq. (11) provides an excellent approximation, as both the RQRPA transition matrix elements and eigenfrequencies closely match the results obtained from the relativistic QFAM.

In practice, once we know the transition matrix elements $\left|\left\langle i\middle|\hat{F}\middle|0\right\rangle\right|^2$, the response function with arbitrary smearing γ larger than 0.01 MeV can be calculated using the empirical formula:

$$R(\omega) \approx \sum_i \frac{\mathrm{d}B(\omega)}{\mathrm{d}\omega}\pi\gamma\Big|_{\omega=\Omega_i,\gamma=0.01} \frac{\Gamma/\pi}{(\omega-\Omega_i)^2+\Gamma^2}, \tag{12}$$

where Γ is the Lorentz width in the RQRPA calculation. In Fig. 2, we present a comparison of the photon absorption cross section for ^{142}Nd calculated by QFAM using γ =0.5 MeV and 1.0 MeV, alongside TSA results obtained with γ=0.01 MeV. The solid lines represent the relativistic QFAM calculations, whereas the dashed lines correspond to the photon absorption cross sections computed using the TSA method. As shown in the figure, the TSA results closely matched the relativistic QFAM calculations, demonstrating the effectiveness of the approximation. Neither $\gamma = 1.00$ MeV nor 0.50 MeV accurately reproduces the experimental data.

3 Calculations and discussion

The photon absorption cross sections of Nd isotopes were first measured in 1971 by Carlos et al., [52]. In this study, we employed the relativistic QFAM method to calculate the photon absorption cross sections for even–even Nd isotopes.

First, we solved the RHB equation using the DD-PC1 relativistic density functional combined with a separable pairing interaction to calculate the ground state properties of even–even Nd isotopes. In Fig. 3, we compare the quadrupole deformations between the experimental data [53] and those obtained from the RHB calculations for ^{142}Nd to ^{152}Nd. Experimentally, the deformation of Nd isotopes increases with neutron number. While the RHB calculations accurately reproduced the deformation for isotopes beyond ^{146}Nd, they predicted ^{142}Nd and ^{144}Nd to be closer to spherical configurations, deviating from the experimental observations.

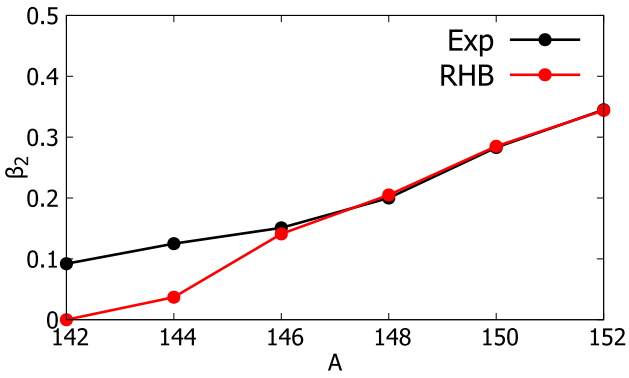

Fig. 3 Comparison of quadrupole deformations between experimental data (black) and RHB calculations (red) for ^{142}Nd to ^{152}Nd

In our previous work [16], we constructed microscopic GDR parameters using relativistic quasiparticle random phase approximation (RQRPA) for spherical nuclei. We now extend this approach by constructing microscopic GDR parameters based on the Dirac Quasiparticle Finite Amplitude Method (relativistic QFAM) combined with the TSA method.

In this study, we introduce an energy-dependent width parameter, defined as

$$\Gamma(\omega) = \delta\Gamma\sqrt{\omega}, \tag{13}$$

where $\delta\Gamma$ is the first parameter to be fitted to experimental data. The photon absorption cross section is then expressed as

$$\sigma(\omega) = \frac{16\pi^3}{9}\frac{e^2}{\hbar c}G \times \omega R(\omega + \delta\omega), \tag{14}$$

where G is the strength parameter used to adjust the height of the cross section and $R(\omega)$ represents the strength function using the TSA method (as defined in Eq.(12)), and $\delta\omega$ accounts for the energy shift. Using the MINUIT package [54], we optimized the three parameters to enhance the relativistic QFAM calculations for the photon absorption cross section of even–even Nd isotopes. As shown in Table 1, the total χ^2 value between the relativistic QFAM results and experimental photon absorption cross sections was reduced by nearly an order of magnitude through the application of the TSA method.

Table 1 Parameters and χ^2 of microscopic GDR parameters with relativistic QFAM and TSA. *C* depicts constant smearing width, *ED* denotes energy-dependent smearing width

Parameters	χ^2	$\delta\Gamma$ (MeV$^{\frac{1}{2}}$)	G	$\delta\omega$ (MeV)
Relativistic QFAM	81.5915	1.0000(C)	–	–
TSA	8.4250	0.4147(ED)	0.9749	0.3276

In Fig. 4, we display the $K^\pi = 0^-$(yellow solid line) and $K^\pi = 1^-$(orange dashed line) components of the photon absorption cross section obtained from the relativistic QFAM calculations with smearing γ=1.0, the total photon absorption cross section obtained from the relativistic QFAM calculations (purple solid line), the results using the TSA method (red solid line), compared with the experimental data [52] and evaluated data of IAEA-2019 [55] or JENDL-5 [56] (black dotted dashed line). Only the JENDL-5 evaluation database predicted the photon absorption cross section of ^{152}Nd.

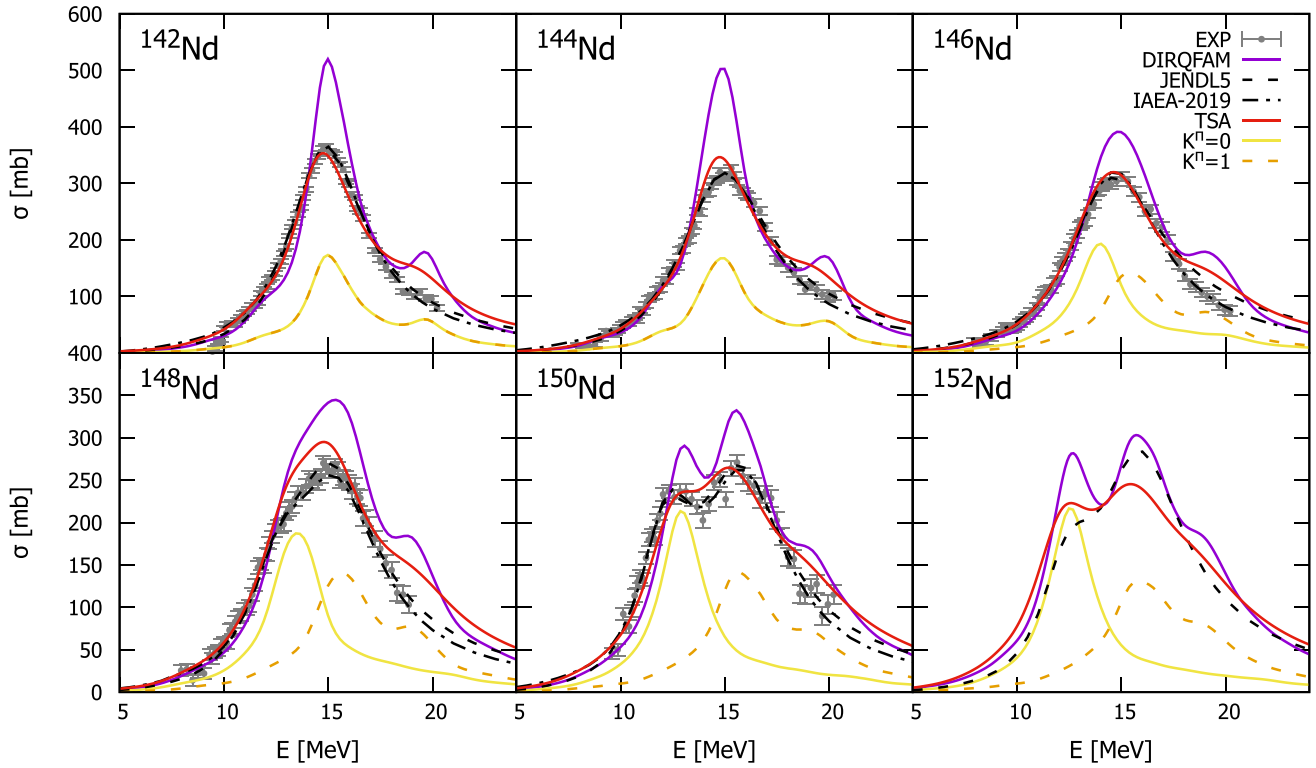

Fig. 4 (Color online) Comparison of relativistic QFAM calculations (purple solid line), the $K^\pi = 0^-$(yellow solid line) and $K^\pi = 1^-$ (orange dashed line) components of the photon absorption cross section and TSA results (red solid line) with experimental photon absorption cross sections (black dots) and evaluated data (black dashed line) for even–even Nd-isotope ranging from ^{142}Nd to ^{152}Nd

As shown in Fig. 4, the centroid energy calculated using relativistic QFAM aligns well with the experimental data. For ^{142}Nd and ^{144}Nd, only a single peak was observed in the photon absorption cross section, as the deformation of these nuclei was minimal. Consequently, the centroid energies of the $K^\pi = 0^-$ and $K^\pi = 1^-$ components were nearly identical. For ^{146}Nd to ^{152}Nd, the $K^\pi = 0^-$ and $K^\pi = 1^-$ components are separated because these nuclei are well deformed. For ^{150}Nd and ^{152}Nd, there are two distinct peaks in the photon absorption cross section owing to splitting of the GDR.

By employing Eqs. (13) and (14), the parameters $\delta\Gamma$, G, and $\delta\omega$ were adjusted by fitting to the experimental data of Carlos et al. [52] for even–even Nd isotopes using the TSA method. This optimization significantly improves the agreement with the experimental data compared to relativistic QFAM calculations. The results demonstrate the effectiveness of the TSA method in accurately reproducing the photon absorption cross sections of Nd isotopes.

Finally, we predicted for ^{152}Nd and compared it with the evaluation data from the JENDL-5 library [56]. Our calculated photon absorption cross sections are significantly smaller than the JENDL-5 data, but are more consistent with the cross sections of ^{150}Nd.

4 Conclusion

In this study, we demonstrated that the GDR strength functions calculated by relativistic QFAM with any appropriate smearing parameter γ can be efficiently obtained using the TSA method. This approach significantly reduces the computational cost of calculating photon absorption cross sections with relativistic QFAM and allows for the incorporation of energy-dependent Lorentzian broadening.

We extend this approach by constructing microscopic GDR parameters based on relativistic QFAM combined with the TSA method, which can describe the photon absorption cross section of even–even Nd isotopes using only three parameters.

In the future, we will broaden our investigation of photon absorption cross sections to include a wider range of atomic nuclei using this TSA method based on relativistic QFAM. Additionally, we will explore the impact of different interactions, such as the density-dependent meson exchange (DD-ME2) parameter set and the pairing strength on the photon absorption cross section.

Acknowledgements We would like to thank Prof. Zhong-Yu Ma (CIAE) and Prof. Peter Ring (TMU) for their insightful discussions on the microscopic calculation of photon strength functions.

Author contributions All authors contributed to the study conception and design. Material preparation, data collection and analysis were performed by Hai-Ruo Liu and Yuan Tian. The first draft of the manuscript was written by Hai-Ruo Liu and all authors commented on previous versions of the manuscript. All authors read and approved the final manuscript.

Data availability The data that support the findings of this study are openly available in Science Data Bank at https://cstr.cn/31253.11.sciencedb.j00186.00783 and https://www.doi.org/10.57760/sciencedb.j00186.00783.

Declarations

Conflict of interest The authors declare that they have no conflict of interest.

References

1. G. Noguere, J. Tommasi, E. Privas et al., Systematics of Nd cumulative fission yields for neutron-induced fission of ^{235}U, ^{238}U, ^{238}Pu, ^{239}Pu, ^{240}Pu and ^{241}Pu. The Eur. Phys. J. Plus **133**, 99 (2018). https://doi.org/10.1140/epjp/i2018-11926-y
2. G.M. Patton, J.D. Inglis, M.E. Sanborn et al., Stable neodymium isotopic composition of nuclear debris samples. J. Radioanal. Nucl. Chem. **332**, 2715–2723 (2023). https://doi.org/10.1007/s10967-023-08935-z
3. Y.L. Jin, Y. Tian, X. Tao et al., Theoretical calculation for photonuclear reaction of $^{142\text{-}146,148,150}$ Nd. Atomic Energy Sci. Technol. **56**, 896–904 (2022). https://doi.org/10.7538/yzk.2022.youxian.0213 (in Chinese)
4. A. Trench, J.P. Sykes, Rare earth permanent magnets and their place in the future economy. Engineering **6**, 115–118 (2020). https://doi.org/10.1016/j.eng.2019.12.007
5. L. Ciacci, I. Vassura, Z. Cao et al., Recovering the new twin: analysis of secondary neodymium sources and recycling potentials in europe. Resour. Conserv. Recycl. **142**, 143–152 (2019). https://doi.org/10.1016/j.resconrec.2018.11.024
6. H.M.H. Zakaly, Y.S. Rammah, S.A.M. Issa et al., Exploring elastic mechanics and radiation shielding efficacy in neodymium(III)-enhanced zinc tellurite glasses: A theoretical and applied physics perspective. J. Theor. Appl. Phys. **17**, 172344 (2023) https://doi.org/10.57647/J.JTAP.2023.1704.44
7. H.-T. Nyhus, T. Renstrøm, H. Utsunomiya et al., Photoneutron cross sections for neodymium isotopes: toward a unified understanding of (γ, n) and (n, γ) reactions in the rare earth region. Phys. Rev. C **91**, 015808 (2015). https://doi.org/10.1103/PhysRevC.91.015808
8. IAEA, Handbook on Photonuclear Data for Applications Cross-sections and Spectra Final Report of a Co-ordinated Research Project 1996-1999, no.IAEA-TECDOC-1178, IAEA, Vienna, 2020 (2020)
9. B.L. Berman, S. Fultz, Measurements of the giant dipole resonance with monoenergetic photons. Rev. Mod. Phys. **47**, 713 (1975). https://doi.org/10.1103/RevModPhys.47.713
10. P. Carlos, H. Beil, R. Bergere et al., The giant dipole resonance in the transition region for the neodymium isotopes. Nucl. Phys. A **172**, 437–448 (1971). https://doi.org/10.1016/0375-9474(71)90725-1
11. H. Utsunomiya, S. Hashimoto, S. Miyamoto, The γ-ray beam-line at newsubaru. Nucl. Phys. News **25**, 25–29 (2015). https://doi.org/10.1080/10619127.2015.1067539
12. H. Wang, G. Fan, L. Liu et al., Development and prospect of Shanghai Laser Compton Scattering Gamma Source. Nucl. Phys. Rev. (in Chinese) **37**, 53–63 (2020). https://doi.org/10.11804/NuclPhysRev.37.2019043

13. S. Goriely, M. Wiedeking, P. Dimitriou, Updating the photonuclear data library and generating a reference database for photon strength functions, in: Summary Report from the Second Research Coordination Meeting, 16-20 October 2017, Vienna, Austria, 2018 (2018)
14. M. Wiedeking, D. Filipescu, P. Dimitriou, Updating photonuclear data library and generating a reference database for photon strength functions, in: Summary Report from the Third Research Coordination Meeting, 17-21 December 2018, Vienna, Austria, 2019 (2019)
15. T. Kawano, Y. Cho, P. Dimitriou et al., IAEA photonuclear data library 2019. Nucl. Data Sheets **163**, 109–162 (2020). https://doi.org/10.1016/j.nds.2019.12.002
16. Y. Tian, X. Tao, J. Wang et al., Giant dipole resonance parameters from photoabsorption cross-sections. Chin. Phys. C **43**, 114102 (2019). https://doi.org/10.1088/1674-1137/43/11/114102
17. X.-Y. Xu, S.-Q. Fan, Q. Yuan et al., Progress in ab initio in-medium similarity renormalization group and coupled-channel method with coupling to the continuum. Nucl. Sci. Tech. **35**, 215 (2024). https://doi.org/10.1007/s41365-024-01585-0
18. L. Zhou, D.-Q. Fang, S.-M. Wang et al., Structure and 2p decay mechanism of ^{18}Mg. Nucl. Sci. Tech. **35**, 107 (2024). https://doi.org/10.1007/s41365-024-01479-1
19. Y.-M. Wang, Q.-B. Chen, Moments of inertia of triaxial nuclei in covariant density functional theory. Nucl. Sci. Tech. **35**, 183 (2024). https://doi.org/10.1007/s41365-024-01552-9
20. Q.-K. Sun, Y. Zhang, Z.-R. Hao et al., Enhancing reliability in photonuclear cross-section fitting with bayesian neural networks. Nucl. Sci. Tech. **36**, 52 (2025). https://doi.org/10.1007/s41365-024-01611-1
21. R. An, S. Sun, L.G. Cao et al., New quantification of symmetry energy from neutron skin thicknesses of ^{48}Ca and ^{208}Pb. Nucl. Sci. Tech. **35**, 182 (2024). https://doi.org/10.1007/s41365-024-01551-w
22. D. M. Brink, Ph.d. thesis, Oxford University, Oxford, United Kingdom (1955)
23. P. Axel, Electric dipole ground-state transition width strength function and 7-MeV photon interactions. Phys. Rev. **126**, 671 (1962). https://doi.org/10.1103/PhysRev.126.671
24. J. Kopecky, M. Uhl, Test of gamma-ray strength functions in nuclear reaction model calculations. Phys. Rev. C **41**, 1941 (1990). https://doi.org/10.1103/PhysRevC.41.1941
25. J. Kopecky, M. Uhl, R. Chrien, Radiative strength in the compound nucleus ^{157}Gd. Phys. Rev. C **47**, 312 (1993). https://doi.org/10.1103/PhysRevC.47.312
26. S. Mughabghab, C. Dunford, A dipole-quadrupole interaction term in E1 photon transitions. Phys. Lett. B **487**, 155–164 (2000). https://doi.org/10.1016/S0370-2693(00)00792-9
27. S. G. Kadmenskij, V. P. Markushev, V. I. Furman, Radiative widths of neutron resonances and giant dipole resonances. Yad. Fiz. **37**, 277–283 (1983). https://inis.iaea.org/records/bdjp0-46z91
28. S.G. Kadmenskij, I.A. Lomachenkov, A.B. Popov et al., Total radiative widths of neutron resonances and photon dipole strength function of compound-compound gamma transitions. Joint Inst. for Nuclear Research, Dubna (USSR). Lab. of Neutron Physics. Report number JINR-R--4-83-600(1983). https://inis.iaea.org/records/p2t11-0kx71
29. V.A. Plujko, S.N. Ezhov, M.O. Kavatsyuk et al., Testing and improvements of gamma-ray strength functions for nuclear model calculations. J. Nucl. Sci. Technol. **39**, 811 (2002). https://doi.org/10.1080/00223131.2002.10875222
30. P. Ring, P. Schuck, *The Nuclear Many-Body Problem* (Springer, 1980)
31. P. Ring, Z. Yu Ma, N.V. Giai et al., The time-dependent relativistic mean-field theory and the random phase approximation. Nucl. Phys. A **694**, 249–268 (2001). https://doi.org/10.1016/S0375-9474(01)00986-1
32. N. Paar, P. Ring, T. Nikšić, D. Vretenar, Quasiparticle random phase approximation based on the relativistic hartree-bogoliubov model. Phys. Rev. C **67**, 034312 (2003). https://doi.org/10.1103/PhysRevC.67.034312
33. Z.M. Niu, Y.F. Niu, H.Z. Liang et al., Self-consistent relativistic quasiparticle random-phase approximation and its applications to charge-exchange excitations. Phys. Rev. C **95**, 044301 (2017). https://doi.org/10.1103/PhysRevC.95.044301
34. N. Hinohara, M. Kortelainen, W. Nazarewicz, Low-energy collective modes of deformed superfluid nuclei within the finite-amplitude method. Phys. Rev. C **87**, 064309 (2013). https://doi.org/10.1103/PhysRevC.87.064309
35. T. Nakatsukasa, T. Inakura, K. Yabana, Finite amplitude method for the solution of the random-phase approximation. Phys. Rev. C **76**, 024318 (2007). https://doi.org/10.1103/PhysRevC.76.024318
36. T. Inakura, T. Nakatsukasa, K. Yabana, Self-consistent calculation of nuclear photoabsorption cross sections: finite amplitude method with skyrme functionals in the three-dimensional real space. Phys. Rev. C **80**, 044301 (2009). https://doi.org/10.1103/PhysRevC.80.044301
37. H. Liang, T. Nakatsukasa, Z. Niu et al., Feasibility of the finite-amplitude method in covariant density functional theory. Phys. Rev. C **87**, 054310 (2013). https://doi.org/10.1103/PhysRevC.87.054310
38. A. Bjelčić, T. Nikšić, Implementation of the quasiparticle finite amplitude method within the relativistic self-consistent mean-field framework: the program dirqfam. Comput. Phys. Commun. **253**, 107184 (2020). https://doi.org/10.1016/j.cpc.2020.107184
39. A. Bjelčić, T. Nikšić, Implementation of the quasiparticle finite amplitude method within the relativistic self-consistent mean-field framework (II): The program DIRQFAM v2.0.0. Comput. Phys. Commun. **287**, 108689 (2023). https://doi.org/10.1016/j.cpc.2023.108689
40. M.B. Chadwick, P. Obloinský, P.E. Hodgson et al., Pauli-blocking in the quasideuteron model of photoabsorption. Phys. Rev. C **44**, 814–823 (1991). https://doi.org/10.1103/PhysRevC.44.814
41. G. Colò, A novel way to study the nuclear collective excitations. Nucl. Sci. Tech. **34**, 189 (2023). https://doi.org/10.1007/s41365-023-01343-8
42. D. Vretenar, N. Paar, P. Ring et al., Collectivity of the low-lying dipole strength in relativistic random phase approximation. Nucl. Phys. A **692**, 496–517 (2001). https://doi.org/10.1016/S0375-9474(01)00653-4
43. V.V. Varlamov, M.E. Stepanov, V.V. Chesnokov, New data on photoabsorption reaction cross sections. Izvestiya Akademii Nauk. Rossijskaya Akademiya Nauk. Seriya Fizicheskaya **67**, 656–663 (2003). https://inis.iaea.org/records/pxmhz-a1926
44. Y. Tian, Z.-Y. Ma, P. Ring, Separable pairing force for relativistic quasiparticle random-phase approximation. Phys. Rev. C **79**, 064301 (2009). https://doi.org/10.1103/PhysRevC.79.064301
45. D.P. Arteaga, P. Ring, Relativistic random-phase approximation in axial symmetry. Phys. Rev. C **77**, 034317 (2008). https://doi.org/10.1103/PhysRevC.77.034317
46. K. Yoshida, T. Nakatsukasa, Dipole responses in Nd and Sm isotopes with shape transitions. Phys. Rev. C **83**, 021304 (2011). https://doi.org/10.1103/PhysRevC.83.021304
47. T. Nakatsukasa, T. Inakura, K. Yabana, Finite amplitude method for the solution of the random-phase approximation. Phys. Rev. C **76**, 024318 (2007). https://doi.org/10.1103/PhysRevC.76.024318
48. P. Avogadro, T. Nakatsukasa, Finite amplitude method for the quasiparticle random-phase approximation. Phys. Rev. C **84**, 014314 (2011). https://doi.org/10.1103/PhysRevC.84.014314

49. T. Nikšić, D. Vretenar, P. Ring, Relativistic nuclear energy density functionals: adjusting parameters to binding energies. Phys. Rev. C **78**, 034318 (2008). https://doi.org/10.1103/PhysRevC.78.034318
50. Y. Tian, Z.-Y. Ma, P. Ring, A finite range pairing force for density functional theory in superfluid nuclei. Phys. Lett. B **676**, 44–50 (2009). https://doi.org/10.1016/j.physletb.2009.04.067
51. N. Hinohara, M. Kortelainen, W. Nazarewicz, Low-energy collective modes of deformed superfluid nuclei within the finite-amplitude method. Phys. Rev. C **87**, 064309 (2013). https://doi.org/10.1103/PhysRevC.87.064309
52. P. Carlos, H. Beil, R. Bergere et al., The giant dipole resonance in the transition region for the neodymium isotopes. Nucl. Phys. A **172**, 437–448 (1971). https://doi.org/10.1016/0375-9474(71)90725-1
53. B. Pritychenko, M. Birch, B. Singh et al., Tables of E2 transition probabilities from the first 2^+ states in even-even nuclei. At. Data Nucl. Data Tables **107**, 1–139 (2016). https://doi.org/10.1016/j.adt.2015.10.001
54. F. James, M. Roos, Minuit-a system for function minimization and analysis of the parameter errors and correlations. Comput. Phys. Commun. **10**, 343 (1975). https://doi.org/10.1016/0010-4655(75)90039-9
55. T. Kawano, Y. Cho, P. Dimitriou et al., IAEA photonuclear data library 2019. Nucl. Data Sheets **163**, 109–162 (2020). https://doi.org/10.1016/j.nds.2019.12.002
56. N. Iwamoto, K. Kosako, T. Fukahori, JENDL photo nuclear data file 2016. J. Nucl. Sci. Technol. **60**, 911–922 (2023). https://doi.org/10.1080/00223131.2022.2161657